Chapter 7
3D Engineering of Ocular Tissues for Disease Modeling and Drug Testing

M. E. Boutin, C. Hampton, R. Quinn, M. Ferrer, and M. J. Song

Abstract The success rate from investigational new drug filing to drug approval has remained low for decades despite major scientific and technological advances, and a steady increase of funding and investment. The failure to demonstrate drug efficacy has been the major reason that drug development does not progress beyond phase II and III clinical trials. The combination of two-dimensional (2D) cellular in vitro and animal models has been the gold standard for basic science research and preclinical drug development studies. However, most findings from these systems fail to translate into human trials because these models only partly recapitulate human physiology and pathology. The lack of a dynamic three-dimensional microenvironment in 2D cellular models reduces the physiological relevance, and for these reasons, 3D and microfluidic model systems are now being developed as more native-like biological assay platforms. 3D cellular in vitro systems, microfluidics, self-organized organoids, and 3D biofabrication are the most promising technologies to mimic human physiology because they provide mechanical cues and a 3D microenvironment to the multicellular components. With the advent of human-induced pluripotent stem cell (iPSC) technology, the 3D dynamic in vitro systems further enable extensive access to human-like tissue models. As increasingly complex 3D cellular systems are produced, the use of current visualization technologies is limited due to the thickness and opaqueness of 3D tissues. Tissue-clearing techniques improve light penetration deep into tissues by matching refractive indices among the 3D components. 3D segmentation enables quantitative measurements based on 3D tissue images. Using these state-of-the-art technologies, high-

M. E. Boutin · M. Ferrer
National Center for Advancing Translational Sciences (NCATS), Rockville, MD, USA

C. Hampton · R. Quinn
National Eye Institute (NEI), Bethesda, MD, USA

M. J. Song (✉)
National Center for Advancing Translational Sciences (NCATS), Rockville, MD, USA

National Eye Institute (NEI), Bethesda, MD, USA
e-mail: minjae.song@nih.gov

© Springer Nature Switzerland AG 2019

K. Bharti (ed.), *Pluripotent Stem Cells in Eye Disease Therapy*,
Advances in Experimental Medicine and Biology 1186,
https://doi.org/10.1007/978-3-030-28471-8_7

throughput screening (HTS) of thousands of drug compounds in 3D tissue models is slowly becoming a reality. In order to screen thousands of compounds, machine learning will need to be applied to help maximize outcomes from the use of cheminformatics and phenotypic approaches to drug screening. In this chapter, we discuss the current 3D ocular models recapitulating physiology and pathology of the back of the eye and further discuss visualization and quantification techniques that can be implemented for drug screening in ocular diseases.

Keywords 3D in vitro model · Biofabrication · High-throughput screening · Human-induced pluripotent stem cell · Microfluidics · Optic cup · Organoid · Outer blood–retina barrier · Tissue clearing

7.1 Introduction

For years, the pharmaceutical and biotechnology industries have been incorporating major advances in scientific knowledge, "omics", engineering, and computational technologies to discover new disease targets, and develop the next generation of therapeutics. Despite the many scientific and technological advances of the last decades, the success rate from investigational new drug (IND) filing to drug approval has remained very low [1]. Over the past 60 years, the number of approved drug compounds per billion US dollar spent on research has continuously decreased, and the approval of a single drug now costs more than a billion dollars. Success rates have been reported for each phase of clinical trials: phase I (overall, 64%; ophthalmology, 84.8%), phase II (overall, 32%; ophthalmology, 44.6%), phase III (overall, 85.3%; ophthalmology, 77.5%), and Likelihood of Approval (overall, 10%; ophthalmology, 17%) [2, 3]. Most drug failures during phase II (48%) and III (55%) were due to a failure to demonstrate drug efficacy [4]. This high failure rate in drug development is in large part due to the use of overly simplistic in vitro cell assays and in vivo mouse models with limited predictive value during drug discovery.

Two-dimensional (2D) in vitro systems have provided assay models for studying healthy and diseased cellular and molecular mechanisms, and for the discovery of targets and biomarkers. These cellular systems have provided data on cytotoxicity of drugs [5], material for proteome/genome/transcriptome analysis [6], and a platform for gene editing [7]. However, results from these cellular systems must be used with caution because a 2D monoculture environment does not recapitulate the three-dimensional (3D) environment of in vivo tissue. Animal model systems, mostly murine and rabbit systems for ocular pathologies [8] and development [9], have been critical for the understanding of disease biology and drug testing in a more relevant in vivo setting. With the advent of biologics in the pharmaceutical field, these animals have helped establish the efficacy of several anti-vascular endothelial growth factor (VEGF) antibodies for the treatment of wet-form age-related macular degeneration (AMD) as well as other neovascularizing pathologies [10]. The com-

bination of 2D in vitro and in vivo models has been the gold standard for drug development in the preclinical stages. However, due to the many physiological differences between model animals and humans, the results of animal studies often fail to translate to human trials. Humanized animal models have been developed to minimize the discrepancies between species by transfecting human genes or introducing human hematopoietic stem cells (HSCs) into immunodeficient mice, which has produced promising models of human infectious disease [11]. In parallel, the development of co-culture systems containing multiple cell types, in many cases generated using primary or induced pluripotent stem cell (iPSC)-derived cells, has initiated a paradigm shift for in vitro systems, in which researchers have also moved from 2D to 3D assays. Additionally, the field of microfluidics has led to the generation of new in vitro systems by providing mechanochemical cues to 3D cellular components. Hence, two major fields, microfluidics and tissue engineering, are becoming mainstays in the development of 3D in vitro systems by providing dynamic and 3D microenvironments.

Microfluidic "chips" contain micro/mesoscale (100–500 μm width) fluidic channels which provide mechanical cues and a dynamic milieu to cells. One of the first applications of in vitro microfluidics systems was to mimic the vascular system. Vascular endothelial cells (ECs) are exposed to hemodynamic forces in the human physiological system (venous system, 1–6 dyn/cm^2; arterial system, 10–70 dyn/cm^2) [12]. It has been shown that flow shear stress is critical to the structure and function of ECs, according to the study of an EC monolayer within a fluidic channel/chamber. This study showed shear flow-induced cytoskeletal rearrangements and significant mechanotransduction by activating transmembrane proteins (e.g., VEGF receptor, ion channel, integrin, PECAM-1) [13]. The addition of a fluidic channel alongside this "vascular" channel, with a porous membrane separating these two channels, enabled a dynamic co-culture system, so-called "organ-on-a-chip", to study interfaces between two mechanobiological regimes [14, 15]. The addition of hydrogel material in the microfluidic system further advanced the structure of the "vascular" channel by providing a 3D microenvironment where multiple cell types can be introduced. Fibroblasts and pericytes, major stromal cells, have been previously reported to play a crucial role in EC's viability. Fibroblasts secrete not only extracellular matrix (ECM) proteins but also VEGF, which is essential for vessel viability and development [16]. Pericytes, perivascular cells, secrete angiopoietin-1 (ANG-1), which is a ligand of the EC TIE-2 receptor. ANG-1 is a well-known factor involved in the regulation of angiogenesis in human development and pathology [17, 18]. Inclusion of these cells within the hydrogel space promotes EC tube formation and provides the 3D architecture of "vascularized" tissue. The self-assembled tubes of ECs within a fibrin-based hydrogel-filled chamber (~1 mm^2) are connected to the adjacent microfluidic channels where an EC monolayer was performed on the wall. The 3D "vascular" network in the chamber has been successfully perfused through anastomoses between ECs from the chamber and ECs from the adjacent channel. Perfusion and connectivity were confirmed by introducing dextran into the adjacent channels [19–23].

Tissue engineering technologies that bridge the gap between 2D in vitro and in vivo systems have grown rapidly in recent years. Bioprinting is a tissue engineering tool that provides a 3D microenvironment for cell/tissue growth by generally dispensing a mixture of hydrogel with cells, called “bioink”. Rapid, scalable, and reliable fabrication of architecturally and physiologically defined functional human tissues still remains a challenge which bioprinting promises to address by integrating five recently emerging technologies: (1) 3D bioprinters are now available with precise XYZ control to reproducibly fabricate tissues with defined 3D geometries, (2) biomaterial and biocompatible hydrogels are being developed to support the 3D structure of tissue-embedded cells, (3) bioreactors are now being designed to deliver mechanical and chemical cues to the cells seeded in the printed tissue, (4) it is also now possible to obtain autologous cells from patients, including human iPSCs, and finally, (5) the ability to quantitatively characterize the morphology and functionality of printed tissues is also now possible using noninvasive technologies such as high-resolution fluorescence confocal/multiphoton microscopy and image analysis techniques.

In ophthalmology, while there are multiple 3D systems currently available, few studies have demonstrated applications of the systems which mimic human ocular physiology. In this chapter, we discuss current options to 3D model ocular tissues using the aforementioned technologies and to authenticate engineered ocular tissues. We further discuss the current challenges in modeling diseases and drug screening of ocular diseases.

7.2 3D Modeling of the Back of the Eye: Outer Blood–Retina Barrier

7.2.1 Background

The back of the eye is a light-sensing layered tissue composed of neurosensory retina, retinal pigment epithelium (RPE), and choroid. Given its unique structure and location between the choroid and retina, the RPE acts as a major homeostatic unit, regulating both choroid and retina tissues. For example, the RPE phagocytoses shed photoreceptor rod outer segments to protect retina, forms tight junctions to prevent large molecules from infiltrating into retina from the blood, and secretes growth factors in a polarized manner to maintain choriocapillaris. Pigment epithelial derived factor (PEDF), an antiangiogenic factor, is predominantly secreted in the apical region, whereas VEGF, a proangiogenic factor, is predominantly secreted in the basolateral region [24–26]. Imbalance of the secretion pattern is thought to initiate choroidal neovascularization (CNV), which is the pathological condition of excessive growth of choriocapillaris toward RPE. RPE cell death debilitates its phagocytic capability, which maintains the viability of photoreceptors. RPE cell death also breaks the mechanical integrity of the RPE barrier by disrupting

intercellular junctional proteins such as ZO-1, occludin, cadherins, and β-catenin [27]. The disruption of intercellular junctions disturbs apicobasal polarity, which regulates the microenvironment of both apical and basal sides by controlling the secretion of distinct molecules at each side. It has been previously reported that, once tight junction and cell polarity are disrupted, the protein secretion pattern of the RPE and the microenvironment of choriocapillaris and photoreceptors are significantly changed [26].

7.2.2 3D Modeling of the Back of the Eye: Engineered Systems

Hamilton et al. showed RPE–EC interactions in an outer BRB model by forming a monolayer of ARPE-19 on one side of an amniotic membrane and forming an HUVEC monolayer on the other side of the membrane in a transwell format [28]. The model demonstrated barrier function, as measured by transepithelial electrical resistance (TEER), and EC fenestration, which is a key feature of choriocapillaris, by transmission electrical microscopy (TEM). Increasing the complexity of the choroid tissue, Chung et al. developed a model containing 3D vascularized "choroid" tissue within a microfluidic channel adjacent to two additional channels [23]. Acellular fibrin-based hydrogel was introduced in the middle channel providing spaces for angiogenesis from the "vascular" channel and facilitating quantification of angiogenesis toward RPE cells (ARPE-19) of the third channel. By increasing VEGF concentration (10–100 ng/ml) in the RPE channel, directional angiogenesis toward the RPE channel was demonstrated. Although the method of creating the VEGF gradient was not physiologically relevant, this was the first model mimicking CNV of wet AMD. The model was further tested with therapeutic intervention using an anti-VEGF drug, Bevacizumab (0.3 mg/ml), which is the gold standard for treatment of CNV [23]. Permeability was assessed by GFP and RFP dextrans to EC and RPE channels, respectively.

We recently developed an outer BRB model using bioprinting technology with iPSC-derived ECs and RPEs (Fig. 7.1). The iPSC technology provides extensive access to human cells as it enables the reprogramming of human somatic cells into pluripotent stem cells. Bioprinting of the fibrin-based gel containing fibroblasts, pericytes, and iPSC-derived ECs, called "bioink", formed choroid-like 3D vascularized tissue on an electrospun biodegradable polymer scaffold. The scaffold provided mechanical support to the bioprinted tissue until stromal cells secreted sufficient amounts of ECM proteins. Human iPSC-derived RPE cells formed a monolayer on the other side of the scaffold. This model demonstrated fenestrated capillaries, and barrier function was assessed by measuring TEER [29, 30, 31].

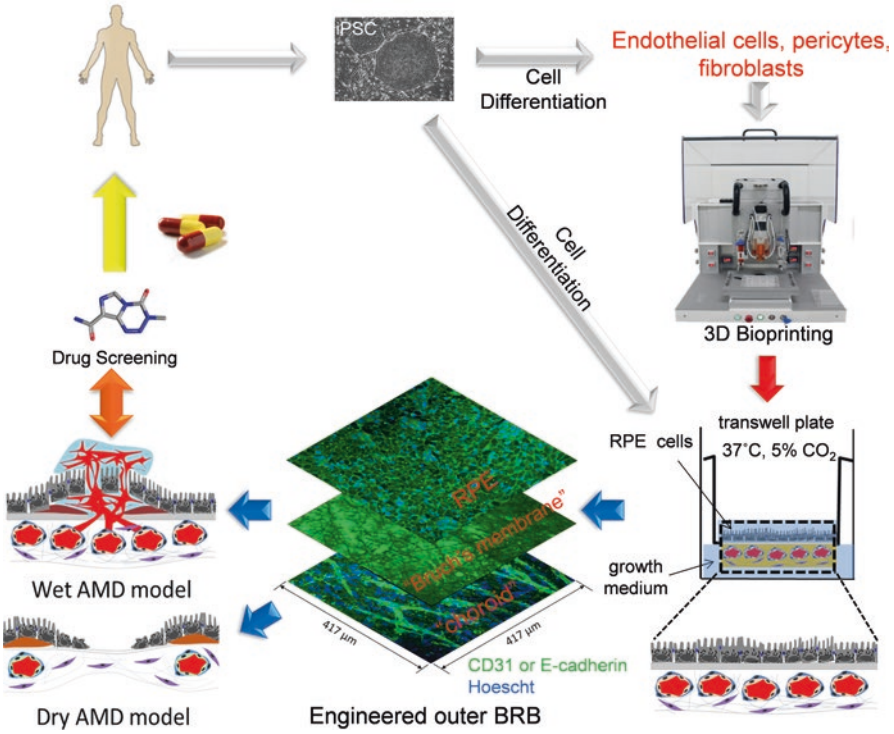

Fig. 7.1 3D Bioprinting of outer BRB using iPSC derived cells: modeling age related macular degeneration for drug discovery

7.2.3 3D System Validation

During the visual cycle, 11-cis-retinal is photoisomerized to all-trans-retinol in photoreceptors. In RPE cells, all-trans-retinol is reversed to 11-cis-retinal by retinoid isomerohydrolase (RPE 65), and the converted 11-cis-retinal is transferred to the photoreceptor for phototransduction. RPE 65 is widely used for identifying RPE, and this can validate RPE location within the engineered BRB tissue. Polarized morphology of RPE can be confirmed by immunostaining for Ezrin, which is a linker protein between the plasma membrane and cytoskeleton. Ezrin expression is localized on the apical region of RPE when it is fully polarized. RPE tight junctions are the major contributor to RPE barrier function, and tight junctions of the RPE can be visualized by ZO-1, Occludin, and Claudin19. TEM visualizes apical processes, polarization, pigmentation, basal infolding, and tight junctions. Barrier function of the RPE monolayer can be assessed by measuring TEER or permeability of dextran [23, 32, 33].

Bruch's membrane is the basement membrane located between RPE and choroid. Bruch's membrane is composed of multiple layers of ECM: RPE basal lamina,

inner collagenous layer, elastic layer, outer collagenous layer, and choriocapillaris basal lamina [34]. Since it consists of multiple types of ECM, the presence of the essential ECM components for in vitro models need to be confirmed.

Choriocapillaris is a key component in the choroid for gas exchange and nutrient delivery. The fenestrated features of choriocapillaris leads to extensive gas exchange between RPE and blood. The fenestration can be tested by expression of the fenestration marker, fenestrated endothelial cell linked protein (FELS). However, the expression of FELS does not provide sufficient evidence of fenestrated morphology. Visualization of ultrastructure by electron microscope is suggested for the final confirmation [35]. EC biomarkers such as PECAM-1, VE-cadherin, and Isolectin-B4 can be used to visualize 3D tube formation. 3D reconstruction of confocal images or histological cross sections can confirm the hollow structure of the EC tubes.

7.3 3D Modeling of the Back of the Eye: Pluripotent Stem Cell-Derived 3D Retina Organoids

7.3.1 Background

Both classical experiments and recent progress in embryology have offered insight into the genetic underpinnings of the stepwise development of the eye and neurosensory retina. Greater understanding within this body of knowledge in conjunction with advances in stem cell technology (specifically the generation of iPSCs [36]) has provided opportunities to engineer signaling cascades for the differentiation of pluripotent cells. In this way, it becomes possible to model various developmental stages of the neurosensory retina.

Developmentally, the eyes are bilateral extensions of diencephalon that begin as optic cups on day 23 of gestation. Between day 25–35, these optic cups evaginate and extend toward overlying surface ectoderm through mesenchyme [37]. Inductive signaling occurs here between the optic vesicle and the surface ectoderm, which eventually becomes the lens placode. More superficial surface ectoderm is fated to become cornea. This evaginating optic vesicle has dorsal-ventral pattern specification, with RPE developing dorsally, optic stalk developing ventrally, and neurosensory retina between the two. Subsequent invagination of the optic vesicle and lens placode leads to formation of the bilayered optic cup, which begins to resemble the ultimate shape of the eye. At this time point, the regions of presumptive neural retina and RPE that were bipotential start to become fated. RPE and neural retina patterning occurs over week 5, with neurogenesis thereafter. Progenitors rapidly proliferate with subsequent differentiation, migration, and organization from weeks 7 to 24. Ganglion cells, cones, and horizontal cells are first to appear first while rods, bipolar cells, and muller glia come later. Development of one cell type leads to production of the subsequent types in sequence secondary to local signaling mechanisms. Maturation and outer segment formation appears from weeks 18 to 28.

This process is mediated by a self-regulatory transcriptional network. Eye-field transcription factors include PAX6, RX, LHX2, SIX3, and SIX6 [38], with expression of OTX2 preceding neural induction. Activin-like factor induces microphthalmia-associated transcription factor (MITF) and RPE specification, while activation of the ERK pathway via fibroblast growth factor (FGF) from the lense ectoderm induces VSX2 (CHX10) and SOX2, promoting retinal development. Simultaneously, transcriptional repression limits the potentiality as development proceeds.

7.3.2 Pluripotent Stem Cell-Derived Optic Cup

With the use of factors to manipulate the signaling cascades associated with these networks, it becomes possible to manipulate the fates of stem cells in culture. There has been significant progress in both 2D and 3D culture methods for obtaining cells fated to a retinal lineage. For example, high efficiencies (80%) of retinal progenitor cells (primarily ganglion and amacrine cells) can be generated from human embryonic stem cells (ESCs) by first antagonizing the bone morphogenic protein (BMP) and Wnt pathways while treating with IGF-1, then treating with FGF [39]. This method resulted in expression of CRX, the earliest known photoreceptor marker, in 10 days of culture. The genetic profile of cells cultured under these conditions showed an accelerated rate of maturation, with 25 days of culture resembling that of the human fetal day 91 retina.

Inhibition of Wnt and Nodal before treatment with retinoic acid and taurine in a stepwise fashion allows increasing maturity, specifically identification of rods and cones [40]. With this culture method, by day 35, around 15% of colonies express RX and PAX6. CRX expression was observable within progenitor colonies by day 90; however, extension of the culture duration to 120 and 170 days led to increasing expression of CRX and mature markers like rhodopsin, recoverin, red/green opsin, and blue opsin. Manipulation of the culture conditions, and exposing cells to antagonists and cytokines that direct pluripotent cells to a ventral, eye field, and photoreceptor specific fates, results in higher differentiation efficiencies [41]. Further modification, with the use of RGD hydrogels can increase optic vesicle formation within embryoid bodies [42].

Even greater maturation of retinas-in-a-dish was demonstrated with the self-organizing optic cups from both mouse and human ESCs [43, 44]. With a serum-free culture of embryoid body-like aggregates with quick aggregation and a basement membrane component, which is either matrigel or laminin and entactin [later replaced with a transient BMP4 treatment, [45]], aggregates of stem cells can become stratified retinal tissue in a dish. Slight modifications to the protocol developed for mouse ESC (high knockout serum replacement enhancing retinal epithelium formation, Wnt inhibition to prevent caudalization, and addition of fetal bovine serum and sonic hedgehog to augment retinal differentiation) allow for human ESCs to form homogenous stem cell aggregates that first form hollow spheres.

These latter develop hemispherical vesicles evaginating from the main body that develop into a two-walled optic cup-like structures. Treatment with Wnt agonists to induce RPE differentiation during day 15–18 enhances MITF expression without suppressing CHX10/VSX2 and allows for RPE/neural retina interaction. The distal portion of the vesicle then invaginates from day 19 to 24 expressing VSX2 (CHX10), SIX3, RX, and PAX6, while proximal cells express PAX6, MITV, and OTX2. Treatment with Activin leads to significant increase in RX expression.

Furthermore, these tissues exhibited interkinetic nuclear migration with progenitors maturing into photoreceptors, ganglion cells, bipolar cells, horizontal cells, amacrine cells, and muller glia. Similar to embryogenesis, ganglion cells appeared first around day 24 at the basal zone of the neural retina. CRX-positive photoreceptor progenitors were present in these earlier time points, but relatively sparse. However, by day 60, the engineered retina contained recoverin-expressing photoreceptors that become substantially denser after day 91. Additionally, the rod-specific marker neural retina leucine zipper (NRL) and the early cone marker retinoid X receptor (RXR) gamma appeared after day 126. Further modification of the protocol with removal of antibiotics and feeder cells was later demonstrated to increase maturation, as observed through the formation of outer segment-like structures [46]. Trisecting of aggregates was shown to enhance yield [47], which would be beneficial for potential transplantation procedures as photoreceptor integration has been demonstrated in mouse models [48].

However, even in the absence of exogenous factors, human anterior neuroectodermal ESCs mature into a population expressing eye-field transcription factors. These can subsequently grow into neural rosettes on a laminin-coated culture dish before being lifted and grown as neurospheres, which acquire a retinal fate and developmentally mimic normal retinogenesis [49, 50]. In this stepwise differentiation, pluripotency is rapidly lost. By day 2 of differentiation cells expressed both PAX6 and RX, and by day 10 LHX2, OTX2, and SOX1. Maintenance of the cultures showed increasing MITF expression from day 16 to 37 and coexpression of VSX2 (CHX10) by day 40. Similar to embryonic retinogenesis, these bipotential populations of cells became subsequently fated by day 50, expressing exclusively either MITF or VSX2 (CHX10). CRX, recoverin, and cone-specific opsin were identified within neurospheres by day 80. Electrophysiological testing of recoverin-positive cells showed a current–voltage relationship consistent with mammalian photoreceptors. This culture method supports the endogenous signaling mechanisms that allow for the recapitulation of retinogenesis and maturation of the retina.

Exploitation of these intrinsic cues occurring between stem cells can allow for the generation of mature retinal structures such as the outer segment and behaviors such as responsiveness to light [51]. Culture of pluripotent stem cells in a neural induction medium first leads to development of anterior neuroepithelial cells expressing PAX6 and SOX2 with subsequent LHX2 from retinal progenitors by day 8. Concomitant expression of VSX2 (CHX10) and MITF illustrates the bipotential nature of the progenitors; however, similar to development, these cells become restricted. These regions expressing PAX6, LHX2, RX, and VSX2 (CHX10) segregate to neural retina and those expressing MITF and PAX6 to RPE. The tissue then begins to resemble the

developmental optic cup from day 17 to 25 with subsequent center-to-periphery neurogenesis occurring over days 35–49 with maturation of photoreceptors, amacrine cells, and horizontal cells expressing OTX2, AP2α, and PROX1. Maintenance of the culture until day 147 allows for cells to segregate into a well-organized outer nuclear layer, expressing more mature markers like rod opsin, L/M-opsin, and S-opsin. Outer segments begin to appear around day 175, with cells expressing proteins involved in phototransduction including the α-subunit of rod transducin (GT1α), the α- and β-subunits of the rod cGMP-phosphodiesterase (PDE6αβ), the rod cyclic-nucleotide-gated channel α-subunit and β-subunit, and retinal guanylate cyclase 1. One limitation inherent in using intrinsic cues for retinal differentiation and maturation is the variability in the differentiation capacity of various cell lines. However, the addition of Wnt antagonists enhances the ability of progenitors to self-organize [52] and can allow for more efficient generation of retinal tissue.

Alternative protocols use sheets of human ESCs suspended in matrigel and cultured in suspensions. First, cells are differentiated toward a neural fate with N2B27 medium, then, in the absence of extrinsic patterning cues, mature to retinal progenitor cells that express eye-field transcription factors by day 10 (SIX3, PAX6, RAX, OTX2) and markers of photoreceptor progenitors by day 13 [53, 54]. Cells cultured in this way first form epithelialized cysts, which spontaneously attach to the culture surface. These can be isolated with dispase and grown in suspension during days 12–17 to enrich VSX2 expression. Long-term culture of these organoids results in stratified neural retina with mature photoreceptor markers like rhodopsin and recoverin by day 152, and outer segments by day 187.

There have been a variety of published protocols regarding the differentiation of mature retinal tissue. Key differences between methods include the application of exogenous factors ultimately leading to differences in the ease of the protocol, and the time at which cell types are acquired. All result in the ability to generate mature human retinal tissue for disease modeling, opening the door for new studies in teasing out pathological mechanisms of disease, developing platforms for drug discovery, and ultimately tissue transplantation. In fact, exploratory transplantation procedures in mouse and monkey models have shown some success, with possible host-graft synaptic connections [55] and some recovery of light-responsive behaviors in diseased animals [56].

7.4 Visualization and Quantification of Markers in 3D Tissue Models

7.4.1 Traditional Histology

Historically, assessment of tissue morphology has been performed by collecting thin physical sections of a tissue and staining to improve visualization of the structures of interest. Tissues are sectioned by embedding in a wax paraffin block for paraffin sectioning or optimum cutting temperature medium for cryosectioning. For

visualization of the retinal layers, the most commonly used stain is the colorimetric stain hematoxylin and eosin (H&E), which colors cell nuclei blue and the protein-rich cytoplasm and extracellular matrix shades of pink. Additionally, specific proteins can be labeled through fluorescent immunocytochemical protocols or colorimetric immunohistochemical protocols.

A consideration when performing staining in retinal tissue is the presence of melanin pigmentation within the RPE and choroid layers. This pigment is similarly colored to the commonly used immunohistochemical chromogen DAB (3,3′-Diaminobenzidine), making it difficult to distinguish DAB labeling within pigmented tissues. For immunofluorescently stained samples, pigment may prevent signal collection from pigmented areas by absorbing light. Notably, melanin pigmentation can also interfere with genomic analysis, such as RNA/DNA quantification and the polymerase chain reaction [57, 58]. Due to these challenges, methods have been developed to decrease pigmentation in tissues through melanin bleaching, using chemicals such as potassium permanganate/oxalic acid or dilute hydrogen peroxide. While most of these protocols have been developed for melanin present in skin or melanoma tissue [59, 60], they are also effective in retinal tissue [61, 62]. Melanin bleaching protocols are performed following tissue sectioning, prior to immunostaining protocols.

7.4.2 Tissue Clearing

While traditional histology is effective for visualizing layered tissue morphology such as the retina, it is difficult to understand the 3D organization of a tissue from thin sections. Fluorescent confocal and two-photon imaging provide alternative solutions to acquire 3D images from intact tissues. However, these imaging techniques encounter technical issues due to the opacity of dense tissues. Light scatters as it travels through cellular compartments with different refractive indices and through extracellular matrix. This scattering makes the collection of fluorescent signal during imaging challenging, especially in 3D tissues. While imaging ability varies widely between different tissue types, this scattering phenomenon typically leads to an inability to image deeper than several cell layers into tissues (~50–100 μm). Additionally, in retina and skin, melanin pigmentation absorbs light and further prevents tissue imaging.

Different techniques have been developed to decrease light scattering within 3D samples and increase the amount of fluorescent signal recovered. Optical tissue clearing is a technique that aims to homogenize refractive index mismatches within tissues and decrease scattering caused by extracellular matrix components. During the past 5–10 years, the number of published protocols has dramatically increased, spurred by improvements in microscope objectives and analysis capabilities (for comprehensive reviews, please see [63] and [64]).

Clearing techniques can be broadly grouped into reversible, chemical protocols and irreversible, crosslinking protocols. Within tissues, a large difference in refractive indices exists between proteins and lipid bilayers (RI ~ 1.50, [65]), and cellular com-

partment mediums (RI ~ water 1.33). The reversible chemical clearing protocols aim to decrease the refractive index differential within tissues by incubating in reagents with high refractive indices. Some protocols use high refractive index solutions such as organic solvents (BABB [66]; 3DISCO [67]), or concentrated sugar solutions (SeeDB [68]). Other protocols incubate in high refractive index aqueous solutions and additionally reduce the scattering of lipid and protein components with reagents such as urea and triton X-100 (Scale [69]; ScaleS [70]; CUBIC [71]). The first published crosslinking clearing technique, termed CLARITY, achieves its effect by crosslinking tissue proteins to an acrylamide gel and using detergent to remove tissue lipids, either passively over an extended time scale, or actively by pulling the detergents using electrophoresis [72]. As lipids are one of the main light scattering components of tissues, this method has been successful in enabling imaging deep into different tissue types, and many new protocols have been developed based on this approach [73–76].

The choice of clearing reagent and protocol must be designed carefully, considering characteristics such as the tissue type of interest, the refractive index of the tissue type, sample size, necessary imaging depth, macromolecules of interest, reagent cost, time/throughput requirements, and fluorophore compatibility. For example, for small (<500 μm thickness) tissue samples, the complex and involved steps of the CLARITY acrylamide crosslinking protocols might not be necessary for imaging. To visualize an endogenous fluorophore or fluorescent antibody, some of the organic solvent protocols should be avoided, as they have been shown to quench fluorophores. If the macromolecule of interest is a lipid, the delipidation CLARITY protocols and perhaps the Scale and CUBIC protocols would be avoided, whereas if the macromolecule of interest was a protein, compatibility would need to be checked with the urea-containing Scale protocol. Most protocols take on the order of days-weeks, depending on the protocol and the sample being cleared. Higher-throughput protocols have been developed to clear samples in a shorter time frame with fewer steps [77–80].

As described above, due to the light-absorbing properties of pigmentation found in the RPE and choroid layers, retinal tissue adds an additional hurdle to fluorescent imaging of 3D tissue samples. The aforementioned melanin bleaching strategies for sectioned tissues can also be adapted to 3D retinal tissue and enhance deep tissue imaging [61]. Bleaching protocols are very effective at removing the dark melanin pigmentation; however, in 3D samples, the opaque tissue of the eye remains. To achieve a sample with minimal light scattering, we have found that the combination of bleaching, followed by immunocytochemical staining and optical clearing, results in optically transparent and imageable tissue.

7.4.3 3D Segmentation and Quantification

Improvements in clearing and microscopy technology have led to an increased ability to resolve fine details within 3D samples, and a push to develop more advanced analysis methods for 3D tissues. For screening, the most common measurements

currently taken of 3D tissues are tissue size by brightfield analysis, and overall fluorescence by widefield microscopy, assessments which do not begin to analyze the wealth of 3D information within the tissue structure. Initial work to improve analysis strategies in 3D have begun by improving segmentation of cell nuclei, a task complicated by light scattering and by the differences in resolution between the *x*, *y*, and *z* imaging axes. Several protocols have demonstrated highly accurate segmentation of cell nuclei in 3D samples [81–83]. However, these protocols have not yet been applied to large data sets. In an effort to develop nuclear segmentation protocols that efficiently analyze large data sets, our group recently developed a protocol that combines optical clearing of 3D tissues, high-content imaging, and high-throughput nuclear segmentation analysis [78]. Using this analysis, we performed nuclear segmentation in an automated fashion for a 384-well plate of spheroids in 5–6 h. By creating the analysis such that it can be run in parallel, we also improved the processing speed by analyzing in parallel on hundreds of cloud-based cpu workers. Protocols such as these can be used to analyze nuclear fluorescent signals, for example, markers of DNA damage, promoter activity, and transcription factors and can be built upon to analyze cytosolic labeling.

Machine learning is a type of artificial intelligence that is being rapidly applied within the field of high-content image analysis. These analyses typically use a sample image data set to train, identify patterns, and learn about the data behavior. Based on this control data set, the program then makes predictions on novel data sets. Machine learning methods have been used successfully in 2D data sets, for example, to classify and score cellular subtypes [84]. Ultimately, the combination of 3D segmentation and analysis protocols with innovative machine learning technologies will enable sophisticated analyses that can adapt to different 3D data sets.

7.5 Drug Screening of Ocular Tissue Models

7.5.1 High-Throughput Drug Screening (HTS) with Stem Cell-Derived Ocular Disease Model

The development of 3D ocular tissue models using iPSC-derived cells and clearing/imaging techniques described above provides a unique opportunity to implement drug screening for ocular diseases using assay systems that are more physiologically-relevant. It is expected that using patient iPSC-derived cells in the context of a relevant tissue, where native physiological cell–cell and cell–microenvironment interactions are maintained, will yield drug responses that are more similar to those obtained in humans, and as a consequence, these assays systems will be more predictive of drug responses in clinic. In the field of drug screening, assay robustness, reproducibility, and sample throughput are key aspects that determine the stage in the drug discovery pipeline at which an assay can be used [85]: primary screening of chemically diverse collections for lead identification for

new drug discovery programs (100,000–1 M compounds) and focused collections for drug repurposing or annotated collections for chemical biology studies (1000s compounds); secondary assays for HTS hit validation or optimization during medicinal chemistry efforts (100–1000s compounds); and tertiary assays for lead optimization and validation (10–20s compounds). Assays used for primary screens are in most cases developed in 384- or 1536-well microplate format in order to increase throughput by using laboratory automation, and reduce cost of reagents because of the smaller volumes used. Because large number of cells are needed to implement primary screens (at least 1000–5000 cells per well in 1536-, and 5000–20,000 cells per well in 384-well), cell production, scale-up, homogeneity of the cell population, and stability of responses with passage and time are critical to have robust and scalable cell-based assays. For this reason, cell lines engineered to express reporters such as GFP or luciferase are widely used in primary high-throughput screens. There are many examples of drug screens using iPSC-derived cells, both to increase the efficiency of differentiation protocols as well as for the correction of disease phenotypes [86]. In many cases, these screens use HTS friendly readouts such as cell viability and reporters, which are engineered at the ESC (mostly from transgenic mice) or iPSC stage of the cells.

High content screening (HCS) is the leading methodology to implement this type of phenotypic screen [87, 88], in which the levels of relevant physiological markers of interest are quantitated either by fusing a protein to a fluorescence reporter, or by immunostaining, followed by cell imaging using automated fluorescent microscopes, coupled with data analysis using algorithms designed to quantify one or more specific phenotypes of interest [89]. One example of a reporter screen has been described for the identification of compounds that accelerate photoreceptor differentiation by stimulating expression of CRX and, consequently, its downstream targets [90]. The strategy applied for this HTS was to use a CRXp-GFP H9 human ESC line. This group showed that human ESC can differentiate and self-organize in vitro to 3D retina cultures in a sequential process starting with floating aggregates of human ESC, which form optic vesicles where neural retina and pigment mass develop. Transcriptomics analysis during the process of differentiation and optical cup formation allowed for the identification of specific sets of genes expressed at the different stages of differentiation. With that information, fluorescent reporters controlled by promoters of such genes can help identify defined developmental stage(s) or individual cell types. Expression of CRXp-GFP reporter in differentiating human ESCs provided the reading output for determining whether a compound accelerated photoreceptor differentiation. The group adapted the assay to 1536-well microplate HTS and went on to screen three-focused collections, the library of pharmacologically active compounds (LOPAC, 1280 compounds), a NIH mechanism interrogation plate (MIPE) collection of annotated compounds (1900), and a drug repurposing collection (~ 3000 compounds). The authors indicated the development of a panel of reporter cells at different stages of photoreceptor differentiation for future drug screening. In another example, Fuller et al. [91] described the use of a rhodopsin (Rho)-GFP-engineered primary retinal neuron from transgenic mice to identify molecules that promoted photoreceptor differentiation. In this example, a hRhoGFP knock-in mouse was generated by replacing the mouse rho open reading frame with

a human Rho-GFP fusion construct, thus creating a rhodopsin reporter controlled by native regulatory mechanisms. The primary retinal neurons extracted from the mice were seeded in a 1536-well plate, and after 21 days, photoreceptors in the culture developed bright GFP fluorescence with bright punctate labeled as "peak rhodopsin" objects, believed to be proto-outer segments. This assay was used to screen the LOPAC collection. These are two examples of focused drug screening using ESC- or iPSC-derived cells to identify compounds that enhance differentiation for potential therapeutic use, both as a treatment to induce photoreceptor regeneration in vivo and also as reagents to enhance the production of iPSC-derived cells for cell-based therapies. In the work by Fuller et al. [91], they also describe how the same cell system can be used to screen for compounds that correct a disease phenotype.

A cell viability assay after stress-induced photoreceptor cell death was developed to identify compounds that were neuroprotective by preventing the slow but progressive loss of photoreceptors and thus could be developed as potential treatments for diseases of retinal degeneration. An HTS friendly readout such as CellTiterGlo, which measures cellular ATP as a surrogate of cell viability, was used to screen the LOPAC collection. In a similar approach, Chang et al. [92] reported a cell viability assay using AMD-patient iPSC-derived RPE cells in which damaging oxidative stress was induced with H_2O_2 treatment. Chronic oxidative stress induces RPE damage that is responsible for the aging process and plays a significant role in the pathogenesis of AMD. These patient-derived RPEs with the AMD-associated background (AMD-RPEs) exhibited reduced antioxidant activity compared with normal RPE cells. As a proof of concept, the authors tested a small set of dietary supplements for retinal protection and natural compounds for antioxidant effects using a methyl thiazol tetrazolium (MTT) assay to measure cell viability. Among several screened candidate drugs, curcumin caused the most significant reduction of reactive oxygen species (ROS) in AMD-RPEs and protected these AMD-RPEs from H_2O_2-induced cell death.

7.5.2 3D Organoids: Human iPSC-Derived Retinal Cup

The examples above illustrate the development of ESC or iPSC-derived assay systems that are amenable to drug screening. While there are not yet studies screening collections of compounds using the recently developed 3D retinal cup organoids, there have been reports of work towards the validation of these systems for screening, including developing HTS friendly assays, extensive morphological, physiological, and pharmacological characterization and validation, and streamlining of iPSC production protocols [52]. Several proof-of-concept studies have been published which demonstrate how 3D retinal cup models can be used as systems to discover new therapeutic interventions. In an approach similar to that described above, induced photoreceptor cell death in mouse iPSC-derived 3D retinal organoids (3D-retinas) by 4-hydroxytamoxifen (4-OHT), which induces photoreceptor degeneration in mouse retinal explants, was established, and then a live-cell imag-

ing system to measure degeneration-related properties was developed to quantify the protective effects of representative ophthalmic supplements for treating the photoreceptor degeneration [93]. In this work, GFP expressing optic cups were prepared from mouse Nrl-GFP iPSCs. Real-time measurements of total intensity from the GFP expressing optic cup using an InCuyte Zoom (Essen BioScience, Inc) enabled the quantitation of 4-OHT-induced acute cell death in the ERRβ-expressing rod photoreceptors. In order to validate the pharmacological relevance of this assay, vitamin E, which is a supplement known to prevent 4-OHT-induced photoreceptor cell death, and lutein, astaxanthin, and anthocyanidin, known to have protective effects against light-induced photoreceptor degeneration in mouse native retina, which is considered to model AMD and Retinitis Pigmentosa (RP), were tested. The results confirm that while vitamin E was able to prevent 4-OHT-induced photoreceptor cell death, the other compounds did not, as was expected from their protective effect being for a different photoreceptor degeneration mechanism. In a similar approach, GFP and YFP reporters were engineered in hiPSC cells, and fluorescence reads were used to measure the effects of H_2O_2 ROS induction on the viability of 3D retina organoids, while a mitochondrial membrane potential fluorescent probe was used to quantify the effects of carbonyl cyanide *m*-chlorophenyl hydrazone (CCCP), a mitochondrial uncoupler [94]. This 3D automated reporter quantification (3D-ARQ) assay platform was extensively validated for HTS robustness in a 96-well plate format. In another published work [95], 3D human iPSC-derived optic cups were used as disease models of Leber Congenital Amaurosis (LCA), an inherited retinal dystrophy that causes childhood blindness. In LCA, photoreceptors are especially sensitive to an intronic mutation in the cilia-related gene CEP290, which causes mis-splicing and premature termination. LCA optic cups were created using iPSCs with the common CEP290 mutation. Even though these iPSCs differentiated normally to 3D optic cups and RPE, the highest levels of aberrant splicing and cilia defects were observed in optic cups. In this case, they did not use compounds to validate the pharmacological value of this model but showed that treating the optic cups with an antisense morpholino oligomer effectively blocked aberrant splicing and restored expression of full-length CEP290, restoring normal cilia-based protein trafficking. In this case, the readouts used to quantitate the correctional effect of the morpholino on the disease phenotype were immunostaining and RT-PCR-based, which are complex to implement for drug screening, and therefore, even though the system was validated as disease model that could be corrected with a treatment, efforts will still need to be made to further develop the system for drug screening.

7.5.3 HTS Readouts and Validation

The complex nature of 3D tissue systems, including scale-up of production and complexity of the disease-relevant readouts, limits their adaptation to HTS and sample throughput. These systems are currently limited to hit validation [96], pharmacological validation of the models, and a few focused screens. Most of the reported

3D tissue model screens have used tumor spheroids [97] or patient-derived tumor cells self-organized organoids [98], and have screened small, focused collections of compounds as proof-of-concept screens, in most cases using cell viability assays or "simpler" cell imaging assays, such as measuring size of spheroids or organoids. The challenges of developing information-rich and disease-relevant imaging-based phenotypic HTS assays that are amenable in 3D tissue models have been discussed above and in the literature [99]. As the technical challenges of using fluorescence imaging-based assays in 3D tissue settings are being addressed [78], one should not forget to consider alternative assays that might be still disease-relevant and amenable to HTS. That includes label-free morphology-based imaging, which coupled to machine learning computational approaches has been used to score for cell differentiation phenotypes in 2D [100–103]. Measuring different morphological features of disease iPSC-derived 3D optic cups using bright-field may enable drug screening for a relatively large collection of compounds, which could provide a smaller set of compounds to study in more complex, information-rich assays. In addition, sampling tissue supernatant for disease-relevant markers such as cytokines can also provide HTS-amenable assay readouts, which could be used as a primary screen, again followed by testing a limited number of hits in information-rich, lower throughput assays. In this regard, liquid chromatography-mass spectrometry (LC-MS) and matrix-assisted laser desorption/ionization-mass spectrometry (MALDI-MS) technologies are now available with higher throughput that would enable the "secretome" analysis of supernatant content of normal versus disease 3D tissue models, and perhaps leverage any differences as a HTS readout. It is worth mentioning that, albeit it is a low-throughput read out, MALDI-MS-based imaging of in-tissue sections is becoming a very powerful tool to image biomolecules for which antibodies are not readily available, including lipids [104–106]. As other techniques such as 3D bioprinting are being used to develop layered systems with relevant monolayers (e.g., RPE), measurements such as TEER [107] will enable additional readouts which could be done in at least 96-well microplate format, which should enable focused screens and hit validation. Finally, there are technologies that enable gene expression analysis in HTS settings, including the QuantiGene Plex Gene Expression Assay, the Nanostring technology and the Fluidigm's integrated fluidic circuits' automated PCR technology. An example of the application of one of these technologies to monitor iPSC differentiation to RPE in 96- and 384-well microplate format was reporter by Ferrer et al. [108].

7.5.4 Machine Learning

It is now clear that to maximize the outcome from drug screens using 3D tissue models, the application of machine learning approaches to both cheminformatics [109] and high-content cell imaging assays will be critical [110–113]. The application of machine learning to cheminformatics should allow for the screening of carefully chosen, focused diversity collections to create models of which structural

features in compounds produce the desired activity in the assays, and rounds of compound selection based on the prediction models generated, and testing should be able to generate new leads for chemistry development. In addition, screening of annotated libraries coupled to cheminformatics and genomics information on a system should enable the identification of new targets and pathways involved in a process [114]. An extensive amount of work is being done to apply machine learning approaches to score and predict control versus disease phenotypes from cell imaging assays, including work on photoreceptor outer segment formation [115]. Most of this work has so far been done in 2D systems, and the hope is that with the development of techniques that allow HT cell imaging in 3D, those will be applied to this more complex systems.

References

1. Scannell JW, Blanckley A, Boldon H, Warrington B (2012) Diagnosing the decline in pharmaceutical R&D efficiency. Nat Rev Drug Discov 11(3):191–200
2. Hay M, Thomas DW, Craighead JL, Economides C, Rosenthal J (2014) Clinical development success rates for investigational drugs. Nat Biotechnol 32(1):40–51
3. BIO BaA (2016) Clinical development success rates 2006-2015. BIO, Washington
4. Harrison RK (2016) Phase II and phase III failures: 2013-2015. Nat Rev Drug Discov 15(12):817–818
5. Repetto G, del Peso A, Zurita JL (2008) Neutral red uptake assay for the estimation of cell viability/cytotoxicity. Nat Protoc 3(7):1125–1131
6. Trapnell C et al (2010) Transcript assembly and quantification by RNA-Seq reveals unannotated transcripts and isoform switching during cell differentiation. Nat Biotechnol 28(5):511–515
7. Potter H (2003) Transfection by electroporation. Curr Protoc Mol Biol Chapter 9:Unit 9 3
8. Connor KM et al (2009) Quantification of oxygen-induced retinopathy in the mouse: a model of vessel loss, vessel regrowth and pathological angiogenesis. Nat Protoc 4(11):1565–1573
9. McAvoy JW, Chamberlain CG, de Iongh RU, Hales AM, Lovicu FJ (1999) Lens development. Eye (Lond) 13(Pt 3b):425–437
10. Ferrara N, Hillan KJ, Gerber HP, Novotny W (2004) Discovery and development of bevacizumab, an anti-VEGF antibody for treating cancer. Nat Rev Drug Discov 3(5):391–400
11. Rongvaux A et al (2014) Development and function of human innate immune cells in a humanized mouse model. Nat Biotechnol 32(4):364–372
12. Chiu JJ, Chien S (2011) Effects of disturbed flow on vascular endothelium: pathophysiological basis and clinical perspectives. Physiol Rev 91(1):327–387
13. Li YS, Haga JH, Chien S (2005) Molecular basis of the effects of shear stress on vascular endothelial cells. J Biomech 38(10):1949–1971
14. Huh D et al (2010) Reconstituting organ-level lung functions on a chip. Science 328(5986):1662–1668
15. Huh D, Torisawa YS, Hamilton GA, Kim HJ, Ingber DE (2012) Microengineered physiological biomimicry: organs-on-chips. Lab Chip 12(12):2156–2164
16. Newman AC, Nakatsu MN, Chou W, Gershon PD, Hughes CC (2011) The requirement for fibroblasts in angiogenesis: fibroblast-derived matrix proteins are essential for endothelial cell lumen formation. Mol Biol Cell 22(20):3791–3800
17. Chen JX, Stinnett A (2008) Disruption of Ang-1/Tie-2 signaling contributes to the impaired myocardial vascular maturation and angiogenesis in type II diabetic mice. Arterioscler Thromb Vasc Biol 28(9):1606–1613

18. Wakui S et al (2006) Localization of Ang-1, -2, Tie-2, and VEGF expression at endothelial-pericyte interdigitation in rat angiogenesis. Lab Invest 86(11):1172–1184
19. Moya ML, Alonzo LF, George SC (2014) Microfluidic device to culture 3D in vitro human capillary networks. Methods Mol Biol 1202:21–27
20. Wang X, Phan DTT, George SC, Hughes CCW, Lee AP (2017) 3D anastomosed microvascular network model with living capillary networks and endothelial cell-lined microfluidic channels. Methods Mol Biol 1612:325–344
21. Jeon JS et al (2015) Human 3D vascularized organotypic microfluidic assays to study breast cancer cell extravasation. Proc Natl Acad Sci U S A 112(1):214–219
22. Kim S, Lee H, Chung M, Jeon NL (2013) Engineering of functional, perfusable 3D microvascular networks on a chip. Lab Chip 13(8):1489–1500
23. Chung M et al (2018) Wet-AMD on a chip: modeling outer blood-retinal barrier in vitro. Adv Healthc Mater 7(2)
24. Becerra SP et al (2004) Pigment epithelium-derived factor in the monkey retinal pigment epithelium and interphotoreceptor matrix: apical secretion and distribution. Exp Eye Res 78(2):223–234
25. Saint-Geniez M, Kurihara T, Sekiyama E, Maldonado AE, D'Amore PA (2009) An essential role for RPE-derived soluble VEGF in the maintenance of the choriocapillaris. Proc Natl Acad Sci U S A 106(44):18751–18756
26. Sonoda S et al (2009) Attainment of polarity promotes growth factor secretion by retinal pigment epithelial cells: relevance to age-related macular degeneration. Aging 2(1):28–42
27. Bailey TA et al (2004) Oxidative stress affects the junctional integrity of retinal pigment epithelial cells. Invest Ophthalmol Vis Sci 45(2):675–684
28. Hamilton RD, Foss AJ, Leach L (2007) Establishment of a human in vitro model of the outer blood-retinal barrier. J Anat 211(6):707–716
29. Song MJ, Quinn R, Dejene R, Bharti K (2017) 3D tissue engineered RPE/"choroid" to identify mechanism of AMD-disease initiation and progression. Assoc Res Vis Ophthalmol 58(8):3760–3760
30. Song MJ, Bharti K (2016) Looking into the future: using induced pluripotent stem cells to build two and three dimensional ocular tissue for cell therapy and disease modeling. Brain Res 1638(Pt A):2–14
31. Hampton C et al (2018) Hypoxia of retina pigment epithelium induces type 1 CNV-like morphology within 3D engineered iPSC-RPE/"Choroid" tissues. Invest Ophthalmol Vis Sci 59(9):3272–3272
32. Hotaling NA et al (2016) Nanofiber scaffold-based tissue-engineered retinal pigment epithelium to treat degenerative eye diseases. J Ocul Pharmacol Ther 32(5):272–285
33. Ablonczy Z, Crosson CE (2007) VEGF modulation of retinal pigment epithelium resistance. Exp Eye Res 85(6):762–771
34. Curcio CA, Johnson M (2012) Structure, function, and pathology of Bruch's membrane. Elastic:465–481
35. Baba T et al (2009) Maturation of the fetal human choriocapillaris. Invest Ophthalmol Vis Sci 50(7):3503–3511
36. Takahashi K et al (2007) Induction of pluripotent stem cells from adult human fibroblasts by defined factors. Cell 131(5):861–872
37. Reh TA (2017) The development of the retina. Ryan's Retina. Elsevier, Amsterdam
38. Zuber ME, Gestri G, Viczian AS, Barsacchi G, Harris WA (2003) Specification of the vertebrate eye by a network of eye field transcription factors. Development 130(21):5155–5167
39. Lamba DA, Karl MO, Ware CB, Reh TA (2006) Efficient generation of retinal progenitor cells from human embryonic stem cells. Proc Natl Acad Sci U S A 103(34):12769–12774
40. Osakada F et al (2008) Toward the generation of rod and cone photoreceptors from mouse, monkey and human embryonic stem cells. Nat Biotechnol 26(2):215–224
41. Mellough CB, Sernagor E, Moreno-Gimeno I, Steel DH, Lako M (2012) Efficient stage-specific differentiation of human pluripotent stem cells toward retinal photoreceptor cells. Stem Cells 30(4):673–686

42. Hunt NC et al (2017) 3D culture of human pluripotent stem cells in RGD-alginate hydrogel improves retinal tissue development. Acta Biomater 49:329–343
43. Eiraku M et al (2011) Self-organizing optic-cup morphogenesis in three-dimensional culture. Nature 472(7341):51–56
44. Nakano T et al (2012) Self-formation of optic cups and storable stratified neural retina from human ESCs. Cell Stem Cell 10(6):771–785
45. Kuwahara A et al (2015) Generation of a ciliary margin-like stem cell niche from self-organizing human retinal tissue. Nat Commun 6:6286
46. Wahlin KJ et al (2017) Photoreceptor outer segment-like structures in long-term 3D retinas from human pluripotent stem cells. Sci Rep 7(1):766
47. Volkner M et al (2016) Retinal organoids from pluripotent stem cells efficiently recapitulate retinogenesis. Stem Cell Rep 6(4):525–538
48. Gonzalez-Cordero A et al (2013) Photoreceptor precursors derived from three-dimensional embryonic stem cell cultures integrate and mature within adult degenerate retina. Nat Biotechnol 31(8):741–747
49. Meyer JS et al (2009) Modeling early retinal development with human embryonic and induced pluripotent stem cells. Proc Natl Acad Sci U S A 106(39):16698–16703
50. Meyer JS et al (2011) Optic vesicle-like structures derived from human pluripotent stem cells facilitate a customized approach to retinal disease treatment. Stem Cells 29(8):1206–1218
51. Zhong X et al (2014) Generation of three-dimensional retinal tissue with functional photoreceptors from human iPSCs. Nat Commun 5:4047
52. Luo Z et al (2018) An optimized system for effective derivation of three-dimensional retinal tissue via wnt signaling regulation. Stem Cells 36:1709
53. Zhu Y et al (2013) Three-dimensional neuroepithelial culture from human embryonic stem cells and its use for quantitative conversion to retinal pigment epithelium. PLoS One 8(1):e54552
54. Lowe A, Harris R, Bhansali P, Cvekl A, Liu W (2016) Intercellular adhesion-dependent cell survival and ROCK-regulated actomyosin-driven forces mediate self-formation of a retinal organoid. Stem Cell Rep 6(5):743–756
55. Shirai H et al (2016) Transplantation of human embryonic stem cell-derived retinal tissue in two primate models of retinal degeneration. Proc Natl Acad Sci U S A 113(1):E81–E90
56. Mandai M et al (2017) Autologous induced stem-cell-derived retinal cells for macular degeneration. N Engl J Med 376(11):1038–1046
57. Dorrie J, Wellner V, Kampgen E, Schuler G, Schaft N (2006) An improved method for RNA isolation and removal of melanin contamination from melanoma tissue: implications for tumor antigen detection and amplification. J Immunol Methods 313(1-2):119–128
58. Eckhart L, Bach J, Ban J, Tschachler E (2000) Melanin binds reversibly to thermostable DNA polymerase and inhibits its activity. Biochem Biophys Res Commun 271(3):726–730
59. Chung JY et al (2016) A melanin-bleaching methodology for molecular and histopathological analysis of formalin-fixed paraffin-embedded tissue. Lab Invest 96(10):1116–1127
60. Liu CH et al (2013) Melanin bleaching with dilute hydrogen peroxide: a simple and rapid method. Appl Immunohistochem Mol Morphol 21(3):275–279
61. Kim SY, Assawachananont J (2016) A new method to visualize the intact subretina from retinal pigment epithelium to retinal tissue in whole mount of pigmented mouse eyes. Transl Vis Sci Technol 5(1):6
62. Thanos A et al (2012) Evidence for baseline retinal pigment epithelium pathology in the Trp1-Cre mouse. Am J Pathol 180(5):1917–1927
63. Tainaka K, Kuno A, Kubota SI, Murakami T, Ueda HR (2016) Chemical principles in tissue clearing and staining protocols for whole-body cell profiling. Annu Rev Cell Dev Biol 32:713–741
64. Silvestri L, Costantini I, Sacconi L, Pavone FS (2016) Clearing of fixed tissue: a review from a microscopist's perspective. J Biomed Opt 21(8):081205

65. Jacques SL (2013) Optical properties of biological tissues: a review. Phys Med Biol 58(11):R37–R61
66. Spalteholz W (1914) Über das Durchsichtigmachen von menschlichen und tierischen Präparaten und seine theoretischen Bedingungen, nebst Anhang: Über Knochenfärbung. S. Hirzel, Leipzig
67. Erturk A et al (2012) Three-dimensional imaging of solvent-cleared organs using 3DISCO. Nat Protoc 7(11):1983–1995
68. Ke MT, Fujimoto S, Imai T (2013) SeeDB: a simple and morphology-preserving optical clearing agent for neuronal circuit reconstruction. Nat Neurosci 16(8):1154–1161
69. Hama H et al (2011) Scale: a chemical approach for fluorescence imaging and reconstruction of transparent mouse brain. Nat Neurosci 14(11):1481–1488
70. Hama H et al (2015) ScaleS: an optical clearing palette for biological imaging. Nat Neurosci 18(10):1518–1529
71. Susaki EA, Ueda HR (2016) Whole-body and whole-organ clearing and imaging techniques with single-cell resolution: toward organism-level systems biology in mammals. Cell Chem Biol 23(1):137–157
72. Chung K et al (2013) Structural and molecular interrogation of intact biological systems. Nature 497(7449):332–337
73. Yang B et al (2014) Single-cell phenotyping within transparent intact tissue through whole-body clearing. Cell 158(4):945–958
74. Murray E et al (2015) Simple, scalable proteomic imaging for high-dimensional profiling of intact systems. Cell 163(6):1500–1514
75. Zheng H, Rinaman L (2016) Simplified CLARITY for visualizing immunofluorescence labeling in the developing rat brain. Brain Struct Funct 221(4):2375–2383
76. Phillips J et al (2016) Development of passive CLARITY and immunofluorescent labelling of multiple proteins in human cerebellum: understanding mechanisms of neurodegeneration in mitochondrial disease. Sci Rep 6:26013
77. Kuwajima T et al (2013) ClearT: a detergent- and solvent-free clearing method for neuronal and non-neuronal tissue. Development 140(6):1364–1368
78. Boutin ME et al (2018) A high-throughput imaging and nuclear segmentation analysis protocol for cleared 3D culture models. Sci Rep 8(1):11135
79. Grist SM, Nasseri SS, Poon T, Roskelley C, Cheung KC (2016) On-chip clearing of arrays of 3-D cell cultures and micro-tissues. Biomicrofluidics 10(4):044107
80. Silva Santisteban T, Rabajania O, Kalinina I, Robinson S, Meier M (2017) Rapid spheroid clearing on a microfluidic chip. Lab Chip 18(1):153–161
81. Rajasekaran B, Uriu K, Valentin G, Tinevez JY, Oates AC (2016) Object segmentation and ground truth in 3D embryonic imaging. PLoS One 11(6):e0150853
82. Li L, Zhou Q, Voss TC, Quick KL, LaBarbera DV (2016) High-throughput imaging: focusing in on drug discovery in 3D. Methods 96:97–102
83. Schmitz A, Fischer SC, Mattheyer C, Pampaloni F, Stelzer EH (2017) Multiscale image analysis reveals structural heterogeneity of the cell microenvironment in homotypic spheroids. Sci Rep 7:43693
84. Jones TR et al (2009) Scoring diverse cellular morphologies in image-based screens with iterative feedback and machine learning. Proc Natl Acad Sci U S A 106(6):1826–1831
85. Inglese J et al (2007) High-throughput screening assays for the identification of chemical probes. Nat Chem Biol 3(8):466–479
86. Ko HC, Gelb BD (2014) Concise review: drug discovery in the age of the induced pluripotent stem cell. Stem Cells Transl Med 3(4):500–509
87. Haasen D et al (2017) How phenotypic screening influenced drug discovery: lessons from five years of practice. Assay Drug Dev Technol 15(6):239–246
88. Ursu A, Scholer HR, Waldmann H (2017) Small-molecule phenotypic screening with stem cells. Nat Chem Biol 13(6):560–563

89. Smith K et al (2018) Phenotypic image analysis software tools for exploring and understanding big image data from cell-based assays. Cell Syst 6(6):636–653
90. Kaewkhaw R et al (2016) Treatment paradigms for retinal and macular diseases using 3-D retina cultures derived from human reporter pluripotent stem cell lines. Invest Ophthalmol Vis Sci 57(5):ORSFl1
91. Fuller JA et al (2014) A high content screening approach to identify molecules neuroprotective for photoreceptor cells. Adv Exp Med Biol 801:773–781
92. Chang YC et al (2014) The generation of induced pluripotent stem cells for macular degeneration as a drug screening platform: identification of curcumin as a protective agent for retinal pigment epithelial cells against oxidative stress. Front Aging Neurosci 6:191
93. Ito SI, Onishi A, Takahashi M (2017) Chemically-induced photoreceptor degeneration and protection in mouse iPSC-derived three-dimensional retinal organoids. Stem Cell Res 24:94–101
94. Vergara MN et al (2017) Three-dimensional automated reporter quantification (3D-ARQ) technology enables quantitative screening in retinal organoids. Development 144(20):3698–3705
95. Parfitt DA et al (2016) Identification and correction of mechanisms underlying inherited blindness in human iPSC-derived optic cups. Cell Stem Cell 18(6):769–781
96. Zhou T et al (2017) High-content screening in hPSC-neural progenitors identifies drug candidates that inhibit zika virus infection in fetal-like organoids and adult brain. Cell Stem Cell 21(2):274–283. e275
97. Mathews Griner LA et al (2016) Large-scale pharmacological profiling of 3D tumor models of cancer cells. Cell Death Dis 7(12):e2492
98. Hou S et al (2018) Advanced development of primary pancreatic organoid tumor models for high-throughput phenotypic drug screening. SLAS Discov 23(6):574–584
99. Carragher N et al (2018) Concerns, challenges and promises of high-content analysis of 3D cellular models. Nat Rev Drug Discov 17:606
100. Fujitani M et al (2017) Morphology-based non-invasive quantitative prediction of the differentiation status of neural stem cells. J Biosci Bioeng 124(3):351–358
101. Kobayashi H et al (2017) Label-free detection of cellular drug responses by high-throughput bright-field imaging and machine learning. Sci Rep 7(1):12454
102. Matsuoka F et al (2013) Morphology-based prediction of osteogenic differentiation potential of human mesenchymal stem cells. PLoS One 8(2):e55082
103. Sasaki H et al (2014) Label-free morphology-based prediction of multiple differentiation potentials of human mesenchymal stem cells for early evaluation of intact cells. PLoS One 9(4):e93952
104. Anderson DM et al (2014) High resolution MALDI imaging mass spectrometry of retinal tissue lipids. J Am Soc Mass Spectrom 25(8):1394–1403
105. Deutskens F, Yang J, Caprioli RM (2011) High spatial resolution imaging mass spectrometry and classical histology on a single tissue section. J Mass Spectrom 46(6):568–571
106. Seeley EH, Schwamborn K, Caprioli RM (2011) Imaging of intact tissue sections: moving beyond the microscope. J Biol Chem 286(29):25459–25466
107. Srinivasan B et al (2015) TEER measurement techniques for in vitro barrier model systems. J Lab Autom 20(2):107–126
108. Ferrer M et al (2014) A multiplex high-throughput gene expression assay to simultaneously detect disease and functional markers in induced pluripotent stem cell-derived retinal pigment epithelium. Stem Cells Transl Med 3(8):911–922
109. Lo YC, Rensi SE, Torng W, Altman RB (2018) Machine learning in chemoinformatics and drug discovery. Drug Discov Today 23:1538
110. Horvath P, Wild T, Kutay U, Csucs G (2011) Machine learning improves the precision and robustness of high-content screens: using nonlinear multiparametric methods to analyze screening results. J Biomol Screen 16(9):1059–1067
111. O'Duibhir E et al (2018) Machine learning enables live label-free phenotypic screening in three dimensions. Assay Drug Dev Technol 16(1):51–63

112. Piccinini F et al (2017) Advanced cell classifier: user-friendly machine-learning-based software for discovering phenotypes in high-content imaging data. Cell Syst 4(6):651–655. e655
113. Smith K, Horvath P (2014) Active learning strategies for phenotypic profiling of high-content screens. J Biomol Screen 19(5):685–695
114. Strang BL et al (2018) Identification of lead anti-human cytomegalovirus compounds targeting MAP4K4 via machine learning analysis of kinase inhibitor screening data. PLoS One 13(7):e0201321
115. Fuller JA, Berlinicke CA, Inglese J, Zack DJ (2016) Use of a machine learning-based high content analysis approach to identify photoreceptor neurite promoting molecules. Adv Exp Med Biol 854:597–603